Timing of root barriers controls soil-to-shoot integration of rhizosphere status

Defeng Shen[1], Kathrin Wippel[1,4], Simone Remmel[1], Pengfan Zhang[1], Noah Kuertoes[1], Ulla Neumann[3] Stanislav Kopriva[2,4] and Tonni Grube Andersen[1,4*]

1: Department of Plant-Microbe Interactions, Max Planck Institute for Plant Breeding Research. Carl-von-Linne-Weg 10, 50829, Cologne, Germany.
2: Institute for Plant Sciences, University of Cologne; Zülpicher Str. 47b, 50674 Cologne, Germany
3: Central Microscopy, Max Planck Institute for Plant Breeding Research. Carl-von-Linne-Weg 10, 50829, Cologne, Germany.
4: Cluster of Excellence on Plant Sciences (CEPLAS)

*Corresponding author. Email: tandersen@mpipz.mpg.de

Abstract

In roots, formation of the Casparian strip in the endodermal cell walls provides a means for selective solute movement by blocking apoplastic flow. This is under spatial surveillance by a receptor-ligand system termed the Schengen pathway. However, the physiological purpose of this is not clear, particularly under natural conditions. To address this, we created plants with an earlier onset of Casparian strips uncoupling barrier formation from the Schengen pathway. Within a complex growth setup, we find that this has severe consequences for a healthy microbiota and nitrogen-induced shoot growth, which provides insights into how root barriers integrate rhizosphere status. This creates a need for an updated nutrient use model that includes root barrier timing as an important factor for coordinating responses between above- and belowground tissues.

INTRODUCTION

To survive in highly dynamic surroundings, plants deploy hydrophobic barriers to protect their vital tissues (1). One particularly well-studied barrier is the Casparian strip (CS) which in roots is situated between cells in the vascular-embracing layer known as the endodermis. The CS blocks flow within the extracellular matrix and thereby forces solute uptake to occur selectively across the endodermal plasma membrane (PM) (2), creating an effective filter to exclude unwanted solutes. In most plants, including the model plant *Arabidopsis thaliana* (hereafter Arabidopsis), the CS consists of centrally localized lignified “bands” in the cell walls, guided by the so-called Casparian strip domain (CSD) in the PM (3). The CSD is established in young, differentiating endodermal cells by the CASPARIAN STRIP MEMBRANE PROTEINs (CASPs) and a number of enzymes responsible for lignin polymerization in the apoplast (3, 4). Expression of most genes involved in CS and CSD formation are under direct control of the endodermis-specific R3R2 MYB-class transcription factor MYB36 (5, 6). Besides the CSD, functional barrier establishment is enabled by the Schengen (SGN) pathway - a self-regulating surveillance system which co-occurs with the onset of CS establishment (7-9). The main components of this system are the stele-synthesized CASPARIAN STRIP INTEGRITY FACTOR (CIF) peptide ligands, their receptor-kinase target known as SCHENGEN3/GASSHO1 (SGN3/GSO1) and the downstream kinase SCHENGEN1 (SGN1/PBL15) (7, 8, 10). The SGN pathway is essential for correct CS formation as CIF diffusion across the unsealed endodermis induces activation of a SGN3/SGN1 complex. This results in CSD fusion and establishment of a tight CS, which prevents further diffusion of CIF peptides (7). In mutants where CS function is disrupted (e.g. *myb36* knockouts), a consequent increase in CIF diffusion hyperactivates the SGN pathway and initiates a number of compensatory responses (8). While the immediate downstream targets of the SGN pathway remain unknown, evidence is emerging that it can additionally convey nutritional status to the stele (11) and relay signals to the shoot (12). Thus, the CS-SGN system is an intriguing model to study how spatiotemporal barrier formation is integrated across the whole plant. However, available mutants in the CS-SGN system are limited to defective CS formation that have either de- or over-activated SGN signaling (13). Therefore, the individual and interconnected roles of these systems have so far been problematic to uncouple, especially under complex growth conditions such as natural soil that include microbial communities.

RESULTS

Rewiring MYB36 leads to earlier, SGN-independent Casparian strip formation

To better understand the root endodermal barrier systems, we aimed to create plants with stronger CS formation and thereby study the overall effects of an increased barrier function. We took a semi-synthetic approach to this and rewired CS formation in Arabidopsis by using the promoter region of the direct MYB36 target *CASP1* (5) to drive *MYB36* expression. In principle, this generates a tissue-restricted positive feedback loop where MYB36 induces itself and its downstream targets specifically in endodermal cells that are initiating CSD formation ($MYB36_{Loop}$). We performed whole-root transcriptome analysis of homozygous lines carrying this construct and compared them to the *myb36-2* mutant and the respective parental lines. This demonstrated functionality of this loop since presence of $MYB36_{Loop}$ led to strongly increased expression of both *MYB36* and *CASP1*, which were almost non-detectable in the *myb36-2* mutant (**Fig. 1A**). Within our significance threshold ($q < 0.05$, $|LOG2\ FC| > 2$), a subset of 113 differentially expressed genes

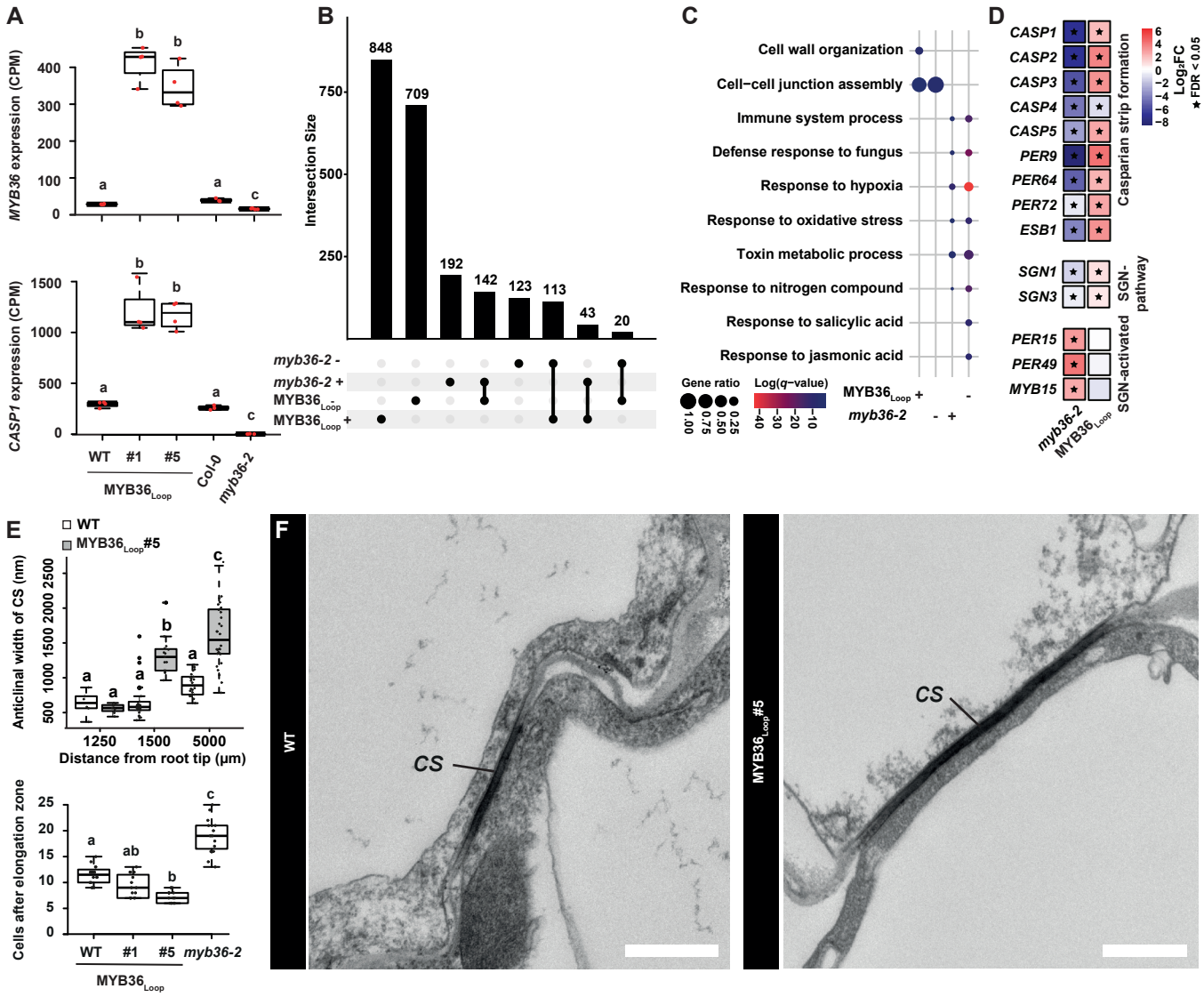

Fig. 1. Transcriptional responses and Casparian strip formation in plants expressing MYB36 driven by the CASP1 promoter. *(A) Read counts of MYB36 and CASP1 (counts per million, CPM). (B) Upset plot depicting differentially expressed genes (DEG) in MYB36Loop and myb36-2 roots compared with the corresponding parental lines. (C) Gene Ontology (GO) term enrichment of DEGs. Gene ratio represents the number of DEGs of GO term divided by the total genes in the GO term. (D) Heatmap depicting expression of individual gene from transcriptome analysis of whole roots. Star symbols represent significantly differentially expressed (FDR < 0.05) genes compared with the corresponding parental lines. (E) Quantification of Casparian strip width in transmission electron microscopy (TEM) images (upper graph) and onset of propidium iodide blockage (lower graph). (F) TEM images of Casparian strips (pointed by black lines) between two endodermal cells, scalebar: 500 nm. For boxplots, the center line indicates median, dots represent data points, the box limits represent the upper and lower quartiles, and whiskers maximum and minimum values. Letters depict statistical difference in a one-way ANOVA analysis with a Holm-Sidak-adjusted posthoc ttest (P < 0.05) (- represent repressed genes, + represent induced genes), CS; Casparian strip. SGN; Schengen.*

(DEGs) showed a similar response pattern as *CASP1* and *MYB36* whereas 142 showed the opposite behavior (i.e., repressed in MYB36$_{Loop}$ and induced in *myb36-2*) (**Fig. 1B**). As expected, when comparing the entire set of DEGs across the two genotypes, the functional gene ontology (GO) term "cell-cell junction assembly" was overrepresented among the induced and repressed DEGs in MYB36$_{Loop}$and *myb36-2*, respectively (**Fig. 1C**). Intriguingly, GO terms related to biotic stress were enriched in the DEGs induced in *myb36-2*, and repressed in MYB36$_{Loop}$ (**Fig. 1C**). This partially overlaps with SGN-induced responses (**Fig. S1A**), suggesting that increased levels of MYB36 in MYB36$_{Loop}$ may directly repress SGN-induced gene expression. However, whereas most known genes involved in CS control (including *SGN1* and *SGN3*) were significantly induced in the MYB36$_{Loop}$ plants, SGN-induced genes such as *PER15/49* and *MYB15* (9, 14) were not affected (**Fig. 1D**). Only one CS-related gene *CASP4* requires both MYB36 and SGN for expression (**Fig. S1B**), and was repressed in the MYB36$_{Loop}$ lines (**Fig. 1D**). Thus, a more likely explanation for the overlap with SGN responses is that spatial coordination of CS onset and CIF diffusion is important for endogenous SGN-induced gene activation. Indeed, introducing the MYB36$_{Loop}$ construct into *sgn3-3* mutants could fully complement the defective CS formation found in this line (10) (**Fig. S1C-D**). Moreover, MYB36$_{Loop}$ lines had an earlier apoplastic blockage (**Fig. 1E**) and the width of the CS was increased from ca. 500 nm in WT to an average of approximately 1500 nm already 1.5 mm from the root tip (**Fig. 1E-F**). None of the MYB36$_{Loop}$ lines showed any significant change in xylem lignification onset nor

ectopic CS formation in adjacent cell types (**Fig. S1F** and **I**). We therefore conclude that positive feedback-driven induction of MYB36 exaggerates the endogenous genetic CS network and overrides the need for SGN signaling to create a functional barrier.

Overloading the Casparian strip domain leads to ectopic CS-like structures

As MYB36$_{Loop}$ lines were made in a *pCASP1::CASP1-GFP* background (3), we set out to describe changes in the dynamics of CS establishment. Onset of CASP1-GFP expression followed a "string-of-pearls" pattern in the anticlinal PM of differentiating endodermal cells (**Fig. 2A**) similar to WT (3, 15). Intriguingly, approximately 2 hours after onset, the CASP1-GFP signal quickly split into two laterally expanding lines and after about 7 hours formed "ring-like" radially expanding patches in the periclinal cell walls (**Fig. 2A-B** and **Movie S1**). These structures, which were not present in WT, contained lignin-specific signals (**Fig. 2B**) and co-occurred with lignifying enzymes normally residing in the CSD although these could be detected in broader ectopic patches (**Fig. S1E**). Additionally, pretreatment with the lignin inhibitor piperonylic acid (PA) (16, 17) led to disturbance in patch assembly (**Fig. 2C**) indicating that lignification is needed for their coherence. Fascinatingly, we found that while MYB36$_{Loop}$ plants had a slight delay of endodermal suberization (**Fig. S1H**) suberin was excluded in the lignified patches within the individual cells (**Fig. 2D**). While treatment with 100 nM CIF2 (9) had no effect on the suberin patterning in MYB36$_{Loop}$ lines, it led to an apparent increase in the size of ectopic lignin patches (**Fig. S1G-H**), which shows that capacity for SGN signaling is still present but the suberization-inducing responses of the SGN pathway (10) are likely overridden by the ectopic MYB36 expression. Combined, our findings support a model where feedback-driven MYB36 expression overloads the CSD with CS-forming machinery (**Fig. 2E**). As a consequence, the cell shows spill-over deposition of lignifying CS-like patches in periclinal cell walls which mimics the formation of the CS-proper and creates an intriguing system to study subcellular mechanisms responsible for CS organization and localization.

Increased Casparian strip formation influences root architecture and signaling

Next, we set out to evaluate how MYB36$_{Loop}$ affects responses to abiotic stress factors. Under standard agar-based growth conditions MYB36$_{Loop}$ lines showed a slight but significant reduction in primary root length (**Fig. 3A, Fig. S2A**). This was accompanied by a strong reduction in lateral root (LR) density similar to what has been described in the *myb36-2* mutant (**Fig. 3B, Fig. S2A**)(18). However, MYB36$_{Loop}$lines showed an earlier repression of primordia development than *myb36-2* (**Fig. S2C**), and these appeared "flattened" against the endodermis rather than dome-shaped as in WT plants (**Fig. S2B**). When subjected to salt or osmotic stress, MYB36$_{Loop}$ plants had improved primary root growth compared to WT plants (**Fig. 3C**). Under standard conditions, MYB36$_{Loop}$ roots displayed increased expression of genes encoding for nitrogen/phosphorus-related stress responses such as *NIN-LIKE-Proteins (NLPs)* as well as a reduction in repressors belonging to the *NITRATE-INDUCIBLE, GARP-TYPE TRANSCRIPTIONAL REPRESSORs*

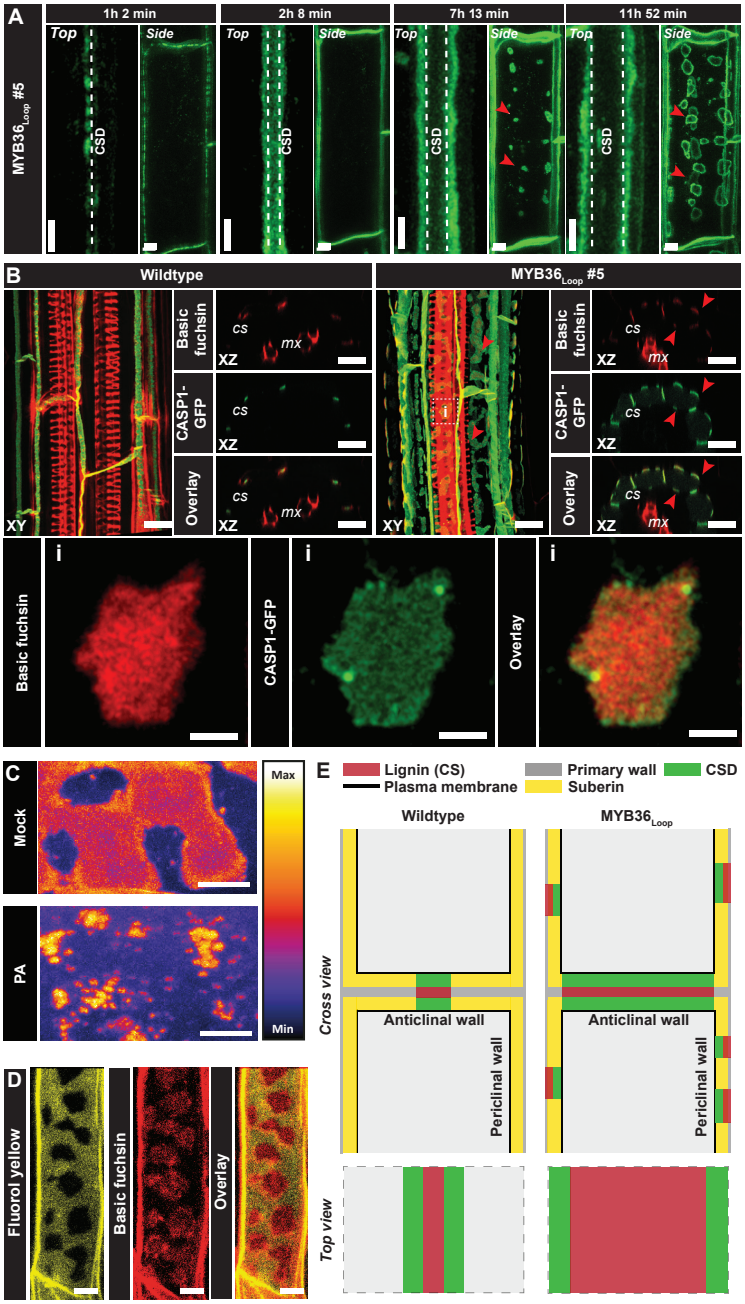

Fig. 2. Analysis of Casparian strip onset and Schengen responses in plants expressing MYB36 driven by the CASP1 promoter. (A) Time course CASP1-GFP expression in MYB36$_{Loop}$#5 plants. Imaging *was initiated in the differentiation zone before onset of CASP1-GFP expression. Images are maximum projection of stacks from the topside of an individual endodermal cell (top) or side view (side). Punctured lines highlight the Casparian strip domain (CSD), red arrowheads point to ectopic CASP1-GFP in the periclinal plasma membrane. (B) Maximum projections of fixed wildtype and MYB36$_{Loop}$#5 roots expressing the CASP1-GFP fusion reporter and stained with Basic fuchsin. For the insert (i) scalebar: 2 µm. (C) Periclinal ectopic CASP1-GFP depositions in MYB36$_{Loop}$#5 roots treated with mock or 10 □M piperonylic acid (PA) for 48 hours. Scalebars: 2 µm. (D) Endodermal cell stained with Basic fuchsin and Fluorol yellow. (E) In wild-type, the CSD and concurrent lignification of the apoplastic space is formed as a centrally localized domain in the anticlinal cell wall. Upon presence of a pCASP1-driven MYB36 expression and establishment of a positive feedback loop, the CSD is widened and overloaded and ectopic CS-like suberin-excluding patches are formed in the periclinal cell walls. Unless otherwise stated, the scalebars represent 10 µm.*

(*NIGTs*) and *BTB AND TAZ DOMAIN PROTEINs (BTs)* families (**Fig. 3D**). Thus, the effects of MYB36$_{Loop}$ on the CS-SGN system may lead to changes in nitrogen-related signaling. When grown in absence of nitrogen (½ MS agar medium without added nitrogen), no significant changes were observed in *myb36-2* plants, whereas MYB36$_{Loop}$ plants showed a significantly increased relative root growth when compared to its parental line (**Fig. 3E**). While no changes were seen in the shoots, a similar root response was seen when phosphorus was omitted but not in the case of sulfur depletion (**Fig.S2D**), suggesting that the improved root growth in MYB36$_{Loop}$ plants is due to changes in nitrogen/phosphorus signaling. As CS establishment has been found to respond to nitrogen status in maize (19), we analyzed the establishment of a functional CS in our mutants under nitrogen restrictive conditions. Remarkably, while WT plants showed a significant dose-dependent delay of functional CS establishment when restricting nitrogen, this was not seen in *myb36-2* nor MYB36$_{Loop}$ plants (**Fig. 3F**). Combined, we propose that early onset of CS formation provides increased resistance to abiotic stresses and brings about a role for the CS-SGN system to affect in particular nitrogen signaling in a way that may be dependent on the timing of apoplastic barrier establishment.

Spatial control of root barriers is crucial for beneficial bacterial associations

As the MYB36$_{Loop}$ roots had reduced expression of genes related to biotic components (**Fig. 1C**), we now investigated if underground biotic associations were affected. For this, we used a soil-based gnotobiotic system where we co-cultivated plants with a synthetic bacterial community (SynCom) consisting of 22 diverse microbial species. In this setup, bacteria-dependent plant growth promotion (PGP) is the read-out of establishment of a beneficial bacterial community (20). After five weeks of growth, both parental lines and the *myb36-2* mutant showed a significant increase in rosette fresh weight in presence of the SynCom (**Fig. 4A**). Excitingly, this was abrogated in MYB36$_{Loop}$ expressing plants (**Fig. 4A**). We observed only minor genotype-dependent changes in the relative abundance of bacterial strains across these lines, including *myb36-2* which has a dysfunctional CS and a hyperactive SGN pathway (5, 6) (**Fig. 4C, Fig. S3A -D**). However, bacterial load, evaluated by levels of bacterial DNA in the roots, was strongly increased in the *myb36-2* plants, but decreased in MYB36$_{Loop}$expressing plants when compared to the parental lines (**Fig. 4B**). Thus, in MYB36$_{Loop}$ expressing plants, potential growth-promoting strains may not reach appropriate numbers to provide the plants with a benefit, or alternatively, other physiochemical factors are missing in this reduced-complexity system. Nevertheless, the lack of PGP indicates that correct coordination of the CS-SGN system is essential for establishing beneficial biotic associations in the roots. To investigate how this translates into natural microbial communities, we grew MYB36$_{Loop}$#5 (which overall displayed a stronger effect than #1) and the *myb36-2* mutant in our local soil (Cologne Agricultural Soil, CAS), and profiled the bacterial and fungal communities associated with the root. Remarkably, and in contrast to the SynCom experiment, under these conditions MYB36$_{Loop}$ roots had an increased bacterial and fungal load, which did not occur in the *myb36-2* mutant (**Fig. 4D**). Moreover,

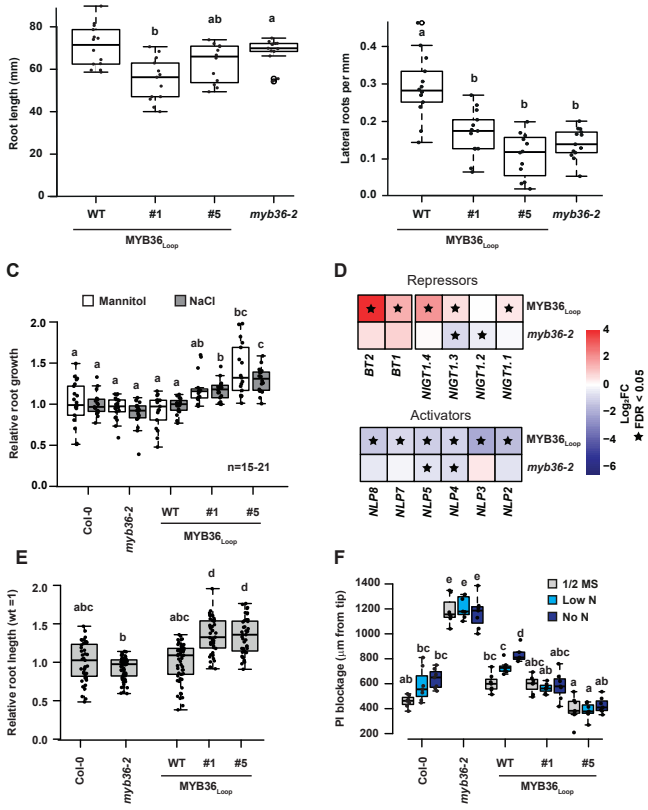

Fig. 3. Root architecture and abiotic stress analysis in mutants with modified Casparian strip formation. *(A) Primary root length of 14-day-old plants from ½ MS agar. (B) Lateral root density of 14-day-old plants grown on ½ MS agar. (C) Relative root growth of 14-day-old plants after 7 days stress conditions (150 mM mannitol or 100 mM NaCl). (D) Heatmap of differentially expressed genes belonging to the BTB AND TAZ DOMAIN PROTEINs (BT), NITRATE-INDUCIBLE, GARP-TYPE TRANSCRIPTIONAL REPRESSORs (NIGT) or NIN-LIKE Protein (NLP) families in MYB36$_{Loop}$and myb36-2 roots. Star symbols represent significantly differential expressed (FDR < 0.05) genes. (E) Relative root growth of 14-day-old plants grown without added nitrogen for 11 days. (F) Onset of functional Casparian strip by means of propidium iodide (PI) blockage. ½ MS agar medium (½MS), 0.11 mM N (Low N) or 0 mM N (No N). For boxplots, the center line in the box indicates median, dots represent data, limits represent upper and lower quartiles, and whiskers maximum and minimum values. Different letters depict statistical difference in a one-way ANOVA analysis with a Holm-Sidak-adjusted posthoc ttest (P < 0.05). #1 and #5 refer to two independent homozygous lines expressing the pCASP1::MYB36 construct in the pCASP1::CASP1-GFP background (WT).*

the alpha diversity of the communities for both bacteria and fungi were strongly reduced in the rhizosphere and roots of MYB36$_{Loop}$ expressing plants (**Fig. 4E**), indicating fewer species being able to colonize the vicinity of those plants. Analysis of the beta-diversity revealed separation of the microbial communities in soil, rhizosphere, and root samples (**Fig. S4A** and **C**), and significantly different community structures on roots according to genotype (**Fig. S4B** and **D**). These differences were caused by a prominent increase or decrease in the relative abundance of several bacterial and fungal families specifically in the

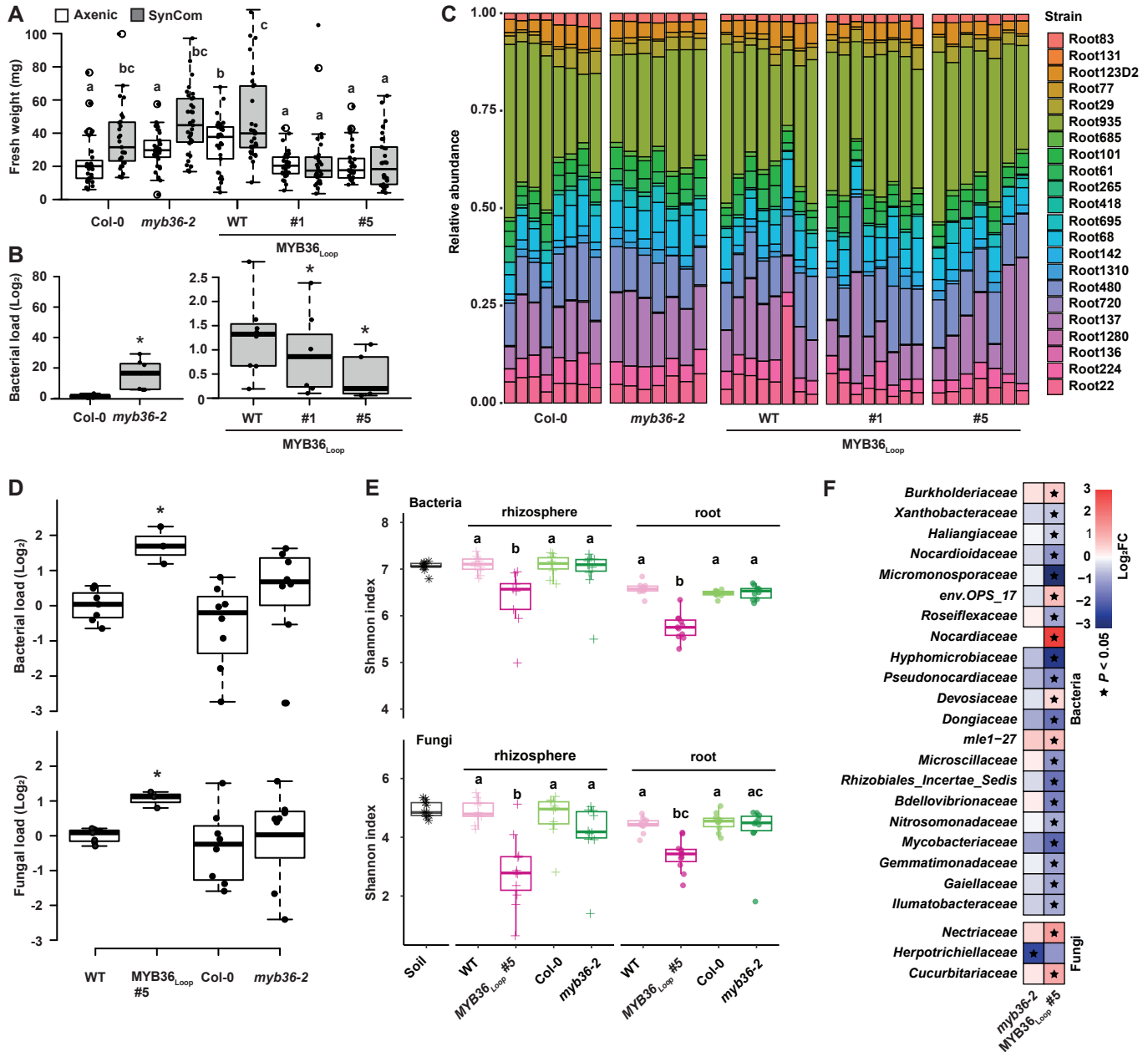

Fig. 4. Analysis of synthetic and naturally occurring microbial communities in roots. *(A) Fresh weight of 5-week-old rosettes with mock treatment (Axenic) or a synthetic bacterial community (SynCom). Letters depict statistical difference in a one-way ANOVA analysis with a Holm-Sidak-adjusted posthoc ttest (P < 0.05). (B) Bacterial load of plants co-cultivated with the SynCom. Asterisks depict significant changes according to a two-sided Student's t-test vs parental line (P < 0.05). (C) Relative abundance of bacteria in roots of 5-week-old plants. (D) Bacterial (upper graph) or fungal (lower graph) load of 4-week-old plants grown under CAS conditions. (E) Alpha diversity of bacterial (upper graph) and fungal (lower graph) communities in soil, root and rhizosphere of pCASP1::CASP1-GFP (WT) , MYB36$_{Loop}$#5, Col-0, and myb36-2 plants grown in CAS. Letters indicate significant differences according to pairwise Wilcoxon rank test with Bonferroni correction. (F) Heatmap depicting bacterial and fungal families in mutant roots compared to corresponding parental lines, based on Log2-transformed fold changes. Stars indicate significant (Wilcoxon test with Bonferroni correction, adjusted P < 0.05) changes. For boxplots, center line indicates the median, dots represent data, box limits upper and lower quartiles, whiskers maximum and minimum values. #1 and #5 refer to two independent homozygous lines expressing the pCASP1::MYB36 construct in the pCASP1::CASP1-GFP background (WT).*

MYB36$_{Loop}$ expressing plants (**Fig. 4F, Fig. S4E** and **G**). In contrast, only minor and mostly non-significant changes were observed in the *myb36-2* communities compared to WT (**Fig. 4E-F** and **Fig. S4F** and **H**). Combined, these analyses reveal that manipulation of the CS-SGN setup has strong effects on biotic interactions in the root, which is likely to impair growth benefits gained from establishing a healthy microbiota.

Spatial coordination of the Casparian strip convey soil status on the shoot ionome

After observing a disturbed root microbiome on CAS, we set out to investigate aboveground effects of distorted endodermal CS-SGN timing and how the soil status influenced this. Independent of soil type, *myb36-2* and MYB36$_{Loop}$ rosettes were significantly smaller than their parental lines (one-way ANOVA, P < 0.05) (**Fig. 5A, Fig.**

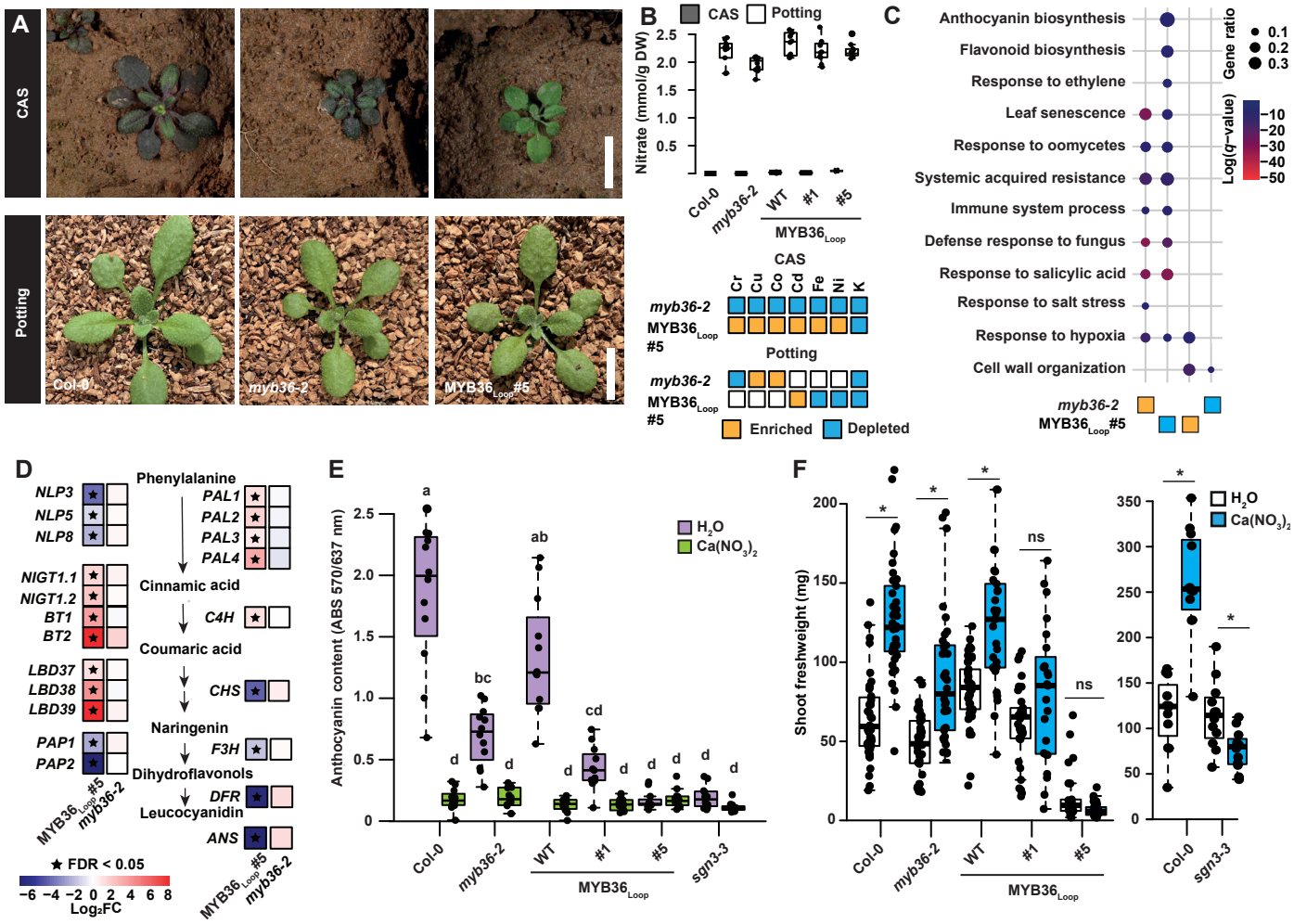

Fig. 5. Shoot analysis of plants with modified root barriers grown in different soil combinations. *(A) Plants grown on Cologne agricultural soil (CAS) or potting conditions (Potting). Scalebars: 1 cm. (B) Nitrate and minerals in rosettes. Minerals are normalized to corresponding parental line (two-sided Student's t-test, P < 0.05). (C) Gene Ontology (GO) enrichment of differentially expressed genes (DEGs) in rosettes from CAS. Gene ratio represents DEGs of GO term divided by total gene number. Orange: up-regulated; blue: downregulated. (D) Heatmap showing behavior of NIN-LIKE-Proteins (NLPs), NITRATE-INDUCIBLE, GARP-TYPE TRANSCRIPTIONAL REPRESSORs (NIGTs), BTB AND TAZ DOMAIN PROTEINs (BTs) families, PRODUCTION OF ANTHOCYANIN PIGMENT 1 and 2 (PAP1 and PAP2) and anthocyanin synthesis genes from CAS. Stars represent significantly changed (FDR < 0.05) genes compared to parental line. (E) Anthocyanin in 4-week-old rosettes from CAS watered with mock (H2O) or nitrate ($Ca(NO_3)_2$). (F) Shoot fresh weight of rosettes from CAS watered with H_2O or nitrate ($Ca(NO_3)_2$). Asterisks depict significant changes between H_2O and nitrate treatments according to a two-sided Student's t-test (P < 0.05). DW; dry weight, ns; not significant. For boxplots, center line in box indicates median, dots represent data, limits represent upper and lower quartiles, and whiskers maximum and minimum values. Letters depict statistical difference of one-way ANOVA with Holm-Sidak-adjusted posthoc ttest (P < 0.05).*

S2E). To investigate if this was associated with changes in elemental composition of the shoot, we profiled the mineral and nutrient content. Indeed, 77.93% of variation in mineral content could be explained by the soil type (**Fig. S5A**). Moreover, $MYB36_{Loop}$ and *myb36-2* rosettes accumulated distinct profiles from each other and their parental lines in both soil conditions (FDR < 0.05) (**Fig. S5A**). Interestingly, on CAS most heavy metals were increased in $MYB36_{Loop}$ plants but decreased in *myb36-2* when compared to their parental lines (**Fig. 5B, Fig. S5B**). This may be a direct effect of the changes in CS status and due to decreased ability to exclude these elements in $MYB36_{Loop}$ expressing plants. Yet, independent of soil type, both $MYB36_{Loop}$ and *myb36-2* rosettes had significantly decreased amounts of potassium (K) compared to the parental line (one-way ANOVA, P < 0.01) (**Fig. 5B, Fig. S5B**). This is intriguing, as previous studies have consistently associated low K accumulation with ineffective barrier formation (10, 13).Yet, this finding indicates that the mechanisms controlling K homeostasis in shoots are likely more complex and may include root-shoot signaling. On CAS, all rosettes had only minute amounts of nitrate compared to potting soil as well as purple coloration in the leaves, while $MYB36_{Loop}$ rosettes remained green (**Fig. 5A-B**). Since the level of other nutrients such as phosphate and sulfate were in a similar range under both conditions (**Fig. S5C**), it is plausible that the disturbed CS-SGN coordination in $MYB36_{Loop}$

roots leads to disturbances in long distance N-signaling. This is supported by the ability of nitrogen-starvation to induce transcriptional responses that lead to increased anthocyanin accumulation (21, 22).

The SGN pathway relays nitrogen signaling to shoots

To obtain a broader view on the CS-SGN dependent nutrient signaling in the shoots, we performed a transcriptional analysis of rosettes from *myb36-2* and $MYB36_{Loop}$#5 as well as their parental lines from different soil types. When comparing SGN-dependent DEGs shared between soil types we found mainly responses related to abscisic acid (ABA) and jasmonic acid (JA) (**Fig. S5D-F**). This has previously been seen as hyperactive SGN mutants have increased ABA-related gene expression in shoots (12). Intriguingly, under CAS conditions, processes related to immunity and leaf senescence were enriched in the genes that were induced in *myb36-2* rosettes and at the same time repressed in $MYB36_{Loop}$ (**Fig. 5C)**, while under potting conditions, these processes where enriched in genes repressed in both genotypes (**Fig. S5D**). Under CAS conditions, functions related to anthocyanin and flavonoid production were specifically enriched in genes repressed in $MYB36_{Loop}$ rosettes (**Fig. 5C**). This was accompanied by a repression of nitrogen-induced genes belonging to the NLP family (23) as well as induction of repressors of the NIGT/BT family (24, 25). In addition, the nitrogen-dependent repressors of anthocyanin production *LATERAL BOUNDARY DOMAIN 37, 38* and *39* (*LBD37,38* and *39*) (26) were induced, whereas their targets, *PRODUCTION OF ANTHOCYANIN PIGMENT 1* and *2 (PAP1* and *PAP2*) (26-28) as well as genes in the anthocyanin biosynthetic pathway (29) were repressed in $MYB36_{Loop}$ when grown on CAS (**Fig. 5D**). Combined the transcriptional responses supports that nitrogen-related signaling is connected to the CS-SGN system. To confirm that this was due to the SGN pathway and not a changed CS establishment, we employed a nitrogen fertilization scheme on CAS and included the *sgn3-3* mutant, with a defective CS and deactivated SGN pathway (10). Interestingly, while the parental and *myb36-2* plants showed a strong decrease in anthocyanin accumulation upon nitrogen supplement (**Fig. 5E**), *sgn3-3* phenocopied the lack of anthocyanin accumulation in $MYB36_{Loop}$ rosettes (**Fig. 5E)**. Moreover, and to our surprise, nitrogen-dependent growth induction was absent in the $MYB36_{Loop}$ plants and excess nitrogen supplementation was in fact repressive for the sgn3-3 mutant (**Fig. 5F**). Combined, these findings propose that under natural, nutrient-scarce conditions, activation of the SGN system in the root provides a mechanism that allows the plant to integrate root and rhizosphere status with shoot responses. Based on the disturbed root communities in $MYB36_{Loop}$ plants grown in CAS, the lack of nitrogen-induced growth promotion may imply an inhibited ability to exploit microbe-associated benefits.

Discussion

In this work, we employed a positive feedback-based tool to generate plants that display accelerated CS onset. Endogenous positive feedback loop-based systems have been identified in secondary cell wall formation (30) and found to play a role in reinforcing robust differentiational outputs in epidermal development (31). These systems must be tightly regulated to avoid run-away expression. While our findings demonstrate that this concept can be employed to dissect redundant genetic networks, it is important to mention that creating an artificial positive transcriptional feedback loop strains the endogenous network either in form of transcriptional co-factor depletion or unspecific repressive mechanisms which may affect outputs of the network investigated. With this in mind, we successfully created a feedback loop that could enhance CS formation and onset. Moreover, while we cannot rule out unspecific effects, we find that plants containing this loop had a number of unexpected, systemic consequences which can be directly ascribed to the CS-SGN mechanism. As the CS onset can respond to nutrients (19) as well as biotic stimuli (13), the spatiotemporal organization of the CS-SGN system represents an elegant mechanism where a nutrient responsive timing of CS onset controls the amount of CIF peptides that can diffuse across the endodermis. This would result in a quantitative activation of the SGN pathway which is directly correlated with functional CS establishment and thereby allows integration of CS status into signaling mechanisms. Indeed, long-distance nitrogen-signaling has been extensively studied in legumes due to the ability to form nitrogen-fixing relationships with rhizobacteria (32). In these systems, upwards movement of peptides conveys signals to shoot responses under low nitrogen availability (33). While these systems are less characterized in Arabidopsis, it is plausible that this may be a downstream target of the SGN system.

Under natural soil conditions, plants with disturbed barrier formation show detrimental growth effects and microbial community composition in roots and shoots (13). However, due to the confounding responses of the SGN-pathway on the overall root barrier formation, the direct roles of the CS and the SGN system has remained unclear. Our work provides a tool capable of addressing the individual as well as coupled effects of CS and SGN systems. Moreover, while this study has given a comprehensive insight into the role of these barriers on mineral accumulation in plant tissues, very little is known of long-distance signaling – in particular with respect to nitrogen – due to technical limitations in the employed analytical setups. Combined, we provide direct and quantitative evidence that beneficial nitrogen-related growth responses require correct coordination of CS-SGN signaling in roots. However, as a microbial disbalance was evident in $MYB36_{Loop}$ expressing plants we cannot rule out that the observed nitrogen-induced growth promotion was due to an inability to establish a healthy root microbiome. This is supported by recent evidence in rice (*Oryza sativa*) where bacterial communities play an important role in nitrogen uptake and usage (34). Nonetheless, our work provides a direct mechanistic link between CS establishment, shoot physiology and microbial community establishment in the rhizosphere. Combined, this work provides quantitative evidence that in a natural environment, timing of the CS onset is essential for establishing a physiological homeostasis in local as well as distal tissues. This forms the basis for a deeper understanding of how plants coordinate its above- and belowground tissues in nature.

MATERIALS AND METHODS

Plant growth

Arabidopsis thaliana ecotype Columbia-0 transgenic and mutant lines were used to perform experiments. Seeds were kept for 2 days at 4 °C in the dark for stratification. For nutrient starvation experiments plants were grown under 16 h light at 21°C and 8 h dark at 19°C vertically on ½ MS medium without sucrose but with distinct nutrient compositions. In all media, the pH was buffered to 5.8 using 10 mM 2-(N-morpholino) ethanesulfonic acid (MES). The following premixed media were used for nutrient starvation assays: Caisson MSP11, MSP44 or MSP21. Low nitrogen conditions were obtained by Caisson MSP21 + 0.037 mM KNO3 + 0.037 mM NH4NO3. For fresh weight shoots and roots of five plants were harvested after 14 days (3 days on ½ MS +11 days on the specified condition). For Cologne agriculture soil (CAS) and potting soil (Blumavis Mini Tray MIM800) experiments, 4-5 plants were grown in 9 x 9 cm square pots in a climate-controlled greenhouse, at 21 °C under a 16 h light/8 h dark regime. For CAS experiments pots were placed on top of a capillary mattress in a tray, and tap water or calcinitTM solution (0.651 g/L, calcinitTM composition: 14.4% nitrate, 1 % ammonium, 26% calcium oxide) (Yara, Germany) was added. For potting soil experiments, soil was moisturized by submerging the pot bottom in water regularly. For gnotobiotic experiments with SynCom inoculation, the FlowPot system was used as previously described (20). The SynCom strains are part of the At-RSPHERE collection (35) and are listed in Table S3.

Cloning

To generate the endodermis-specific feedback loop expression constructs, the coding sequence of MYB36 (5) was Gateway cloned into a pDONR221 entry vector using BP clonase II (Invitrogen) according to manufactures description. Together with previously generated P4L1r pDONR entry vectors containing the pCASP1 sequence (3), this was recombined using LR-clonase II (Invitrogen) into a FastRed selection-containing destination vector (pED97) (36). The final construct was transformed into pCASP1::CASP1-GFP and other backgrounds using the floral dip method and selected using FastRed selection .

Staining procedures

All staining procedures were done using ClearSee staining (37, 38). Briefly, plants were fixed in 3 mL 1 x PBS containing 4 % p-formaldehyde for 1 hour at room temperature and washed twice with 3 mL 1 x PBS. Following fixation, the seedlings were cleared in 3 mL ClearSee solution (10 % xylitol, 15 % sodium deoxycholate and 25 % urea in water) under gentle shaking. After overnight clearing, the solution was exchanged to new ClearSee solution containing 0.2 % Basic Fuchsin and 0.1 % Calcofluor White for lignin and cell wall staining respectively. The dye solution was removed after overnight staining and rinsed once with fresh ClearSee solution. The samples were washed for 30 min with gentle shaking followed by overnight incubation in ClearSee solution before imaging. Suberin staining of Arabidopsis root was performed as previously described (36). In case of combined suberin and basic fuchsin staining the procedure was according to (39). Briefly, vertically grown 5-day old seedlings were incubated in Fluorol Yellow 088 (Sigma) (0.01 %, in lactic acid) and incubated for 30 min at 70 °C. The stained seedlings were rinsed shortly in water and transferred to a freshly prepared solution of aniline blue (0.5 %, in water) for counterstaining. PI assays were done as described (40). PI stained seedlings were washed for 2-3 min in water and transferred to a chambered cover glass (Thermo Scientific), and imaged either using Confocal laser scanning (CLSM) or epifluorescence microscopy. The number of endodermal cells were scored using a Leica DM5500 wide field microscope (from onset of cell elongation defined as endodermal cell length being more than two times than width in the median, until PI could not penetrate into the stele or from the root tip to end of PI penetration).

Microscopy

All confocal images were taken using a Zeiss LSM 980 system. Fluorophore settings were ex 488nm, em 505-550 nm for GFP and Fluorol yellow 088, ex 594 nm, em 610-650 nm for mCherry, ex 561 nm, em 580-600 nm for Basic fuchsin, ex 405 nm em 420-430 nm for Calcofluor white. Airyscan images were taken using the 4Y multiplex setting. FY staining and PI analysis were done on a Zeiss Axiozoom V16 system (GFP filtercube ex: 470 nm/40 em:525/50 bs: 500). For PI TX2 filtercube ex: 560 nm/40 em:645/75 bs: 595 nm).

Transmission electron microscopy

For quantification of the Casparian strip width by TEM, 6-day-old pCASP1::CASP1-GFP and $MYB36_{Loop}$#5 seedlings were placed in small Petri dishes filled with 0.05 M MOPS buffer supplemented with 0.1% Tween20 and 10 mM cerium chloride and incubated with gentle agitation at room temperature. After 30 min, the CeCl3-containing MOPS buffer was replaced by 2.5% glutaraldehyde in 0.05 M phosphate buffer (v/v), pH 7.2, and seedlings were gently agitated for one hour. Subsequently, seedlings were transferred into glass vials filled with 1% osmium tetroxide (EMS, #19150) in 0.05 M phosphate buffer (w/v), pH 7.2, supplemented with 1.5% potassium ferrocyanide, for another hour. After three rinses in water, seedlings were embedded into 2% low melting point agarose and three fragments were sampled from the distal 1.5 cm-long part of the root. Root fragments were then dehydrated with a series of ethanol, gradually transferred into acetone and embedded into Araldite 502/Embed 812 resin (EMS, #13940) using the EMS Poly III embedding machine (EMS, #4444). Ultrathin sections (≈70 nm) were cut at specific distances from the root tip with a Reichert-Jung Ultracut E and collected on Formvar-coated copper slot grids (41). After staining with 0.1% potassium permanganate in 0.1 N H2SO4 for one minute (w/v) followed by 0.5% uranyl acetate in water (w/v) for 10 minutes and lead citrate for 15 min, sections were examined with a Hitachi H-7650 TEM operating at 100 kV and equipped with an AMT XR41-M digital camera. For immunogold detection of CASP1-GFP in $MYB36_{Loop}$ roots were high-pressure frozen in a Leica EM HPM 100 high-pressure freezer between two large aluminum specimen carriers (ø 4.6 mm) enclosing a cavity of 150 µm depth filled with ½ MS medium. After freeze substitution in the Leica EM AFS2 freeze substitution device using 0.5% uranyl acetate in acetone (w/v), bringing samples from -85 °C to -20 °C over seven

days, samples were transferred to ethanol and gradually embedded into LR White resin (Plano GmbH, R1281) at -20 °C over six days with constant agitation. Samples were polymerized in pure LR White resin with UV light for 24 h at -20 °C and 24 h at 0 °C. Ultramicrotomy was performed as described above with the exception that sections were collected on Formvar-coated gold slot grids. Immunogold labelling of CASP1-GFP was carried out according to using a 1:5 dilution of rat monoclonal anti-GFP 3H9 (Chromotek) and a 1:20 dilution of goat anti-rat IgG conjugated to 10 nm colloidal gold particles (British Biocell International). Sections were stained with potassium permanganate and uranyl acetate (no lead citrate) and imaged as described above.

Transcriptomics

For transcriptomic analysis on roots, Col-0, *myb36-2*, pCASP1::CASP1-GFP (WT), $MYB36_{Loop}$#1 and $MYB36_{Loop}$#5 seedlings were grown on standard ½ MS agar medium for seven days. Whole roots were harvested and immediately frozen in liquid nitrogen. RNA was extracted using a TRIzol (Invitrogen)-adapted ReliaPrep RNA extraction kit (Promega) (36). For transcriptomic analysis on CAS soil and potting soil grown shoots, Col-0, *myb36-2*, WT, and $MYB36_{Loop}$#5 seedlings were grown on standard solid ½ MS medium for 7 days, then transferred to CAS soil or potting soil. Whole rosette leaves of 4-week-old plants were harvested and immediately frozen in liquid nitrogen. RNA extractions were performed as mentioned above. RNA quality was determined using a Bioanalyzer 2100 system (Agilent Technologies, USA). Library preparation and paired-end 150 bp sequencing were conducted by Novogene (Cambridge, UK). Approximately 40 million raw reads were generated per sample. RNA-seq raw reads of *sgn3-3* roots were acquired from (9, 14), raw reads of CIF2 treated Col-0 roots dataset (48 hours after CIF2 treatment) were acquired from (9). All raw reads were preprocessed using fastp (v0.22.0)(42). Filtered high-quality reads were mapped to A. thaliana TAIR10 reference genome with Araport 11 annotation (Phytozome genome ID: 447) using HISAT2 (v2.2.1) , and counted using featureCounts from the Subread package (v2.0.1) (43). All statistical analyses were performed using R (v4.1.2) (https://www.R-project.org/). Read counts were transformed to cpm (counts per million) using edgeR package (44). Lowly expressed (less than 0.5 x total sample number (19 for ½ MS roots, 26 for CAS shoots, 16 for potting shoots, 6 for (14) 9 for (9)) cpm over all samples, and at least 1 cpm in n samples (6 for ½ MS roots, 8 for CAS shoots, 5 for potting shoots, 2 for (14), 3 for (9)) genes were removed from the analysis. Differentially expressed genes (DEGs) were identified by pairwise comparisons using the glmFit function in edgeR package (44) with absolute fold change more than 2 and a false discovery rate (FDR) corrected P-value less than 0.05. Note that for root transcriptome analysis, $MYB36_{Loop}$#1 and $MYB36_{Loop}$#5 samples were compiled as one genotype, and compared with WT. Gene Ontology (GO) term enrichment analysis was performed using Metascape (45). Only GO terms with adjusted P value (q-value) lower than 0.05 were considered as significantly enriched. Heatmaps were generated using pheatmap package (https://cran.r-project.org/web/packages/pheatmap/index.html) or ggplot2 package (46). Upset plots were generated using UpSetR package.

CP-MS and IC analysis

The total mineral content was determined by inductively coupled plasma mass spectrometry (ICP-MS) following the method described in (47). Approximately 5 mg of homogenized dried plant material were digested using 500 µL of 67% (w/w) HNO3 overnight at room temperature and subsequently placed in a 95°C water bath for 30 min or until the liquid was completely clear. After cooling to room temperature, the samples were placed on ice and 4.5 mL of deionized water was carefully added to the tubes. The samples were centrifuged at 4°C at 2,000 g for 30 min and the supernatants were transferred to new tubes. The elemental concentration was determined using Agilent 7700 ICP-MS (Agilent Technologies) (47). Inorganic anion (nitrate, phosphate, and sulfate) levels were measured by ion chromatography, as described in (48). Approximately 10 mg of dried plant material was homogenized in 1 mL deionized water, shaken for 1 h at 4°C, and subsequently heated at 95 °C for 15 min. The anions were determined by the Dionex ICS-1100 chromatography system and separated on a Dionex IonPac AS22 RFIC 4× 250 mm analytic column (Thermo Scientific, Darmstadt, Germany), using 4.5 mM Na_2CO_3/1.4 mM $NaHCO_3$ as running buffer (48).To compare the shoot ionomes between different genotypes under different growth conditions, a principal coordinate analysis (PCoA) was performed with a Bray–Curtis dissimilarity index calculated using vegdist() function in the R vegan package (https://github.com/jarioksa/vegan). To assess the variations explained by growth conditions (CAS vs. potting soil), a PERMANOVA testing was performed, based on the Bray–Curtis dissimilarity index, using adonis2() function from the R vegan package with 999 permutations. To assess the statistical difference of shoot ionomes between different genotypes within each growth condition, a pairwise comparison (PERMANOVA) was performed, based on the Bray–Curtis dissimilarity index, using the pairwise.adonis() function in the R pairwise Adonis package (https://github.com/pmartinezarbizu/pairwiseAdonis) with 999 permutations, followed by Benjamini-Hochberg post hoc testing.

Community profiling

For community profiling on CAS grown root samples plants were grown on standard ½ MS agar medium for 7 days, then transferred to CAS soil and grown for three weeks. Three to four plants from the same pot were collected as one replicate. The whole root systems of three to four plants were carefully isolated, rhizosphere and root compartments were harvested as previously described (20). All samples (including unplanted soil samples) were transferred to Lysing Matrix E tubes (FastDNA Spin Kit for Soil, MP Biomedicals), frozen in liquid nitrogen and stored at −80 °C for further processing. DNA was isolated using a FastDNA Spin Kit for Soil (MP Biomedicals), then subjected to bacterial and fungal community profiling, and absolute quantification of bacterial and fungal load, as previously described (49). For community profiling on roots derived from FlowPot experiments, roots of all plants in one FlowPot were harvested as one sample, cleaned from attaching soil particles, and processed

further like described above. Library preparation for amplicon sequencing was performed as described previously (50). Briefly, multiplexing of samples was performed by double-indexing with barcoded forward and reverse oligonucleotides for 16S rRNA gene or fungal ITS amplification. Samples from the FlowPot experiment were sequenced on the Illumina Novaseq platform at Novogene, UK. Samples of the greenhouse experiment in CAS soil were sequenced on our in-house Illumina MiSeq platform. Amplicon data processing was performed as previously described (20). Shortly, the reads were demultiplexed by QIIME2 plugin 'cutadapt demux-paired'(51). Demultiplexed reads were merged with Flash2 (51). For synthetic communities, the merged reads were fed into Rbec (https://github.com/PengfanZhang/Rbec) to profile the microbial communities. For natural communities, reads were fed into DADA2 to generate the ASV table. Chimeras were detected using Vsearch (52) and excluded from the downstream analysis. Taxonomic classification of ASVs were conducted by the Bayesian classifier trained on the SILVA (Ver. 138) and Unite (Ver. 8) for bacteria and fungi respectively (53, 54). All the ASVs assigned to mitochondria and chloroplast were eliminated from the ASV table.

Anthocyanin content measurement

Measurement of anthocyanin content in rosettes grown under CAS or standard potting soil conditions was performed as previously described (55). Absorbances at 530 and 637 nm were measured using Tecan Infinite 200 PRO plate reader.

ACKNOWLEDGEMENTS

All authors thank Bart Boesten, and Ila Rouhara for technical support. Sabine Ambrosius and the Biocenter MS Platform Cologne are thanked for measurements of mineral composition. Ton Timmers and the Central Microscopy facility (CEMIC) are thanked for microscopy aid. Aristeidis Stamatakis and his greenhouse team are thanked for help with plant growth. We moreover thank Meike Burow, Niko Geldner and Magdalena Marek for helpful comments to the manuscript. TGA thanks the Sofja Kovalevskaja programme from the Alexander von Humboldt foundation and the Max Planck Society for funding. TGA would further like to thank BDR and APM for their support in form of much needed liquid aid at timely intervals. Funding: Research in the lab of TGA is supported by the Sofja Kovalevskaja programme from the Alexander von Humboldt foundation and the Max Planck Society. Research in the lab of SK is supported by the Deutsche Forschungsgemeinschaft (DFG) under Germany´s Excellence Strategy – EXC 2048/1 – project 390686111. KW is funded by DFG Priority Programme SPP2125 DECRyPT. Author contributions: Conceptualization: TGA. Methodology: DS, KW, NK, UN, SK, PZ, TGA. Investigation: DS, SR, KW, NK, UN, SK, TGA. Visualization: DS, KW and TGA. Funding acquisition: TGA, SK. Main writing: TGA. All authors read and commented on the final version of the manuscript. Competing interests: All authors declare that they have no competing interests. Data and materials availability: All RNA-seq data generated in this study have been deposited at National Center for Biotechnology Information under BioProject ID PRJNA940103. Raw amplicon sequencing reads will be deposited at the European Nucleotide Archive. Scripts used for data analyses will be available at github.

REFERENCES

1. *N. Geldner, The Endodermis. Annual Review of Plant Biology 64, 531-558 (2013).*

2. *M. Barberon, N. Geldner, Radial Transport of Nutrients: The Plant Root as a Polarized Epithelium. Plant Physiology 166, 528-537 (2014).*

3. *D. Roppolo et al., A novel protein family mediates Casparian strip formation in the endodermis. Nature 473, 380-383 (2011).*

4. *Y. Lee, Maria C. Rubio, J. Alassimone, N. Geldner, A Mechanism for Localized Lignin Deposition in the Endodermis. Cell 153, 402-412 (2013).*

5. *T. Kamiya et al., The MYB36 transcription factor orchestrates Casparian strip formation. Proceedings of the National Academy of Sciences 112, 10533-10538 (2015).*

6. *L. M. Liberman, E. E. Sparks, M. A. Moreno-Risueno, J. J. Petricka, P. N. Benfey, MYB36 regulates the transition from proliferation to differentiation in the Arabidopsis root. Proceedings of the National Academy of Sciences 112, 12099-12104 (2015).*

7. *V. G. Doblas et al., Root diffusion barrier control by a vasculature-derived peptide binding to the SGN3 receptor. Science 355, 280-284 (2017).*

8. *S. Fujita, CASPARIAN STRIP INTEGRITY FACTOR (CIF) family peptides - regulator of plant extracellular barriers. Peptides 143, 170599 (2021).*

9. *S. Fujita et al., SCHENGEN receptor module drives localized ROS production and lignification in plant roots. The EMBO Journal 39, e103894 (2020).*

10. *A. Pfister et al., A receptor-like kinase mutant with absent endodermal diffusion barrier displays selective nutrient homeostasis defects. eLife 3, e03115 (2014).*

11. *F.-L. Wang et al., A potassium-sensing niche in Arabidopsis roots orchestrates signaling and adaptation responses to maintain nutrient homeostasis. Developmental Cell 56, 781-794.e786 (2021).*

12. *P. Wang et al., Surveillance of cell wall diffusion barrier integrity modulates water and solute transport in plants. Scientific Reports 9, 4227 (2019).*

13. *I. Salas-González et al., Coordination between microbiota and root endodermis supports plant mineral nutrient homeostasis. Science 371, (2021).*

14. *G. Reyt et al., Two chemically distinct root lignin barriers control solute and water balance. Nature Communications 12, 2320 (2021).*

15. K. Hématy, D. De Bellis, X. Wang, A. P. Mähönen, N. Geldner, Analysis of exocyst function in endodermis reveals its widespread contribution and specificity of action. Plant Physiology 189, 557-566 (2022).

16. T. G. Andersen et al., Tissue-autonomous phenylpropanoid production is essential for establishment of root barriers. Current Biology 31, 965-977. e965 (2021).

17. M. Schalk et al., Piperonylic acid, a selective, mechanism-based inactivator of the trans-cinnamate 4-hydroxylase: A new tool to control the flux of metabolites in the phenylpropanoid pathway. Plant Physiol 118, 209-218 (1998).

18. M. Fernández-Marcos et al., Control of Arabidopsis lateral root primordium boundaries by MYB36. New Phytologist 213, 105-112 (2017).

19. Y. Guo et al., Nitrogen supply affects ion homeostasis by modifying root Casparian strip formation through the miR528-LAC3 module in maize. Plant Commun, 100553 (2023).

20. K. Wippel et al., Host preference and invasiveness of commensal bacteria in the Lotus and Arabidopsis root microbiota. Nature Microbiology 6, 1150-1162 (2021).

21. L. Chalker-Scott, Environmental significance of anthocyanins in plant stress responses Photochemistry and Photobiology 70. (1999).

22. C. Diaz et al., Leaf yellowing and anthocyanin accumulation are two genetically independent strategies in response to nitrogen limitation in Arabidopsis thaliana. Plant and Cell Physiology 47, 74-83 (2006).

23. M. Konishi, S. Yanagisawa, Arabidopsis NIN-like transcription factors have a central role in nitrate signalling. Nature communications 4, 1617 (2013).

24. V. Araus et al., Members of BTB gene family of scaffold proteins suppress nitrate uptake and nitrogen use efficiency. Plant Physiology 171, 1523-1532 (2016).

25. T. Kiba et al., Repression of nitrogen starvation responses by members of the Arabidopsis GARP-type transcription factor NIGT1/HRS1 subfamily. The Plant Cell 30, 925-945 (2018).

26. G. Rubin, T. Tohge, F. Matsuda, K. Saito, W.-R. d. Scheible, Members of the LBD Family of Transcription Factors Repress Anthocyanin Synthesis and Affect Additional Nitrogen Responses in Arabidopsis The Plant Cell 21, 3567-3584 (2009).

27. D. D. Rowan et al., Environmental regulation of leaf colour in red 35S: PAP1 Arabidopsis thaliana. New Phytologist 182, 102-115 (2009).

28. N. Li et al., The heterologous expression of Arabidopsis PAP2 induces anthocyanin accumulation and inhibits plant growth in tomato. Functional & integrative genomics 18, 341-353 (2018).

29. H. K. Dooner, T. P. Robbins, R. A. Jorgensen, Genetic and developmental control of anthocyanin biosynthesis. Annual review of genetics 25, 173-199 (1991).

30. M. Taylor-Teeples et al., An Arabidopsis gene regulatory network for secondary cell wall synthesis. Nature 517, 571-575 (2015).

31. Y. H. Kang et al., The MYB23 gene provides a positive feedback loop for cell fate specification in the Arabidopsis root epidermis. Plant Cell 21, 1080-1094 (2009).

32. P. Gautrat, C. Laffont, F. Frugier, S. Ruffel, Nitrogen Systemic Signaling: From Symbiotic Nodulation to Root Acquisition. Trends in Plant Science 26, 392-406 (2021).

33. S. Roy, L. M. Müller, A rulebook for peptide control of legume–microbe endosymbioses. Trends in Plant Science 27, 870-889 (2022).

34. J. Zhang et al., NRT1.1B is associated with root microbiota composition and nitrogen use in field-grown rice. Nature Biotechnology 37, 676-684 (2019).

35. Y. Bai et al., Functional overlap of the Arabidopsis leaf and root microbiota. Nature 528, 364-369 (2015).

36. T. G. Andersen et al., Diffusible repression of cytokinin signalling produces endodermal symmetry and passage cells. Nature 555, 529-533 (2018).

37. D. Kurihara, Y. Mizuta, Y. Sato, T. Higashiyama, ClearSee: a rapid optical clearing reagent for whole-plant fluorescence imaging. Development 142, 4168-4179 (2015).

38. R. Ursache, T. G. Andersen, P. Marhavý, N. Geldner, A protocol for combining fluorescent proteins with histological stains for diverse cell wall components. Plant J 93, 399-412 (2018).

39. M. Sexauer, D. Shen, M. Schön, T. G. Andersen, K. Markmann, Visualizing polymeric components that define distinct root barriers across plant lineages. Development 148, (2021).

40. S. Naseer et al., Casparian strip diffusion barrier in Arabidopsis is made of a lignin polymer without suberin. Proceedings of the National Academy of Sciences 109, 10101-10106 (2012).

41. D. T. Moran, J. C. Rowley. (1987).

42. S. Chen, Y. Zhou, Y. Chen, J. Gu, fastp: an ultra-fast all-in-one FASTQ preprocessor. Bioinformatics 34, i884-i890 (2018).

43. Y. Liao, G. K. Smyth, W. Shi, The R package Rsubread is easier, faster, cheaper and better for alignment and quantification of RNA sequencing reads. Nucleic Acids Res 47, e47 (2019).

44. M. D. Robinson, D. J. McCarthy, G. K. Smyth, edgeR: a Bioconductor package for differential expression analysis of digital gene expression data. Bioinformatics 26, 139-140 (2009).

45. Y. Zhou et al., Metascape provides a biologist-oriented resource for the analysis of systems-level datasets. Nature Communications 10, 1523 (2019).

46. H. Wickham, ggplot2:Elegant Graphics for Data Analysis. Use R! (Springer Cham, 16 June 2016), vol. XVI, pp. 260.

47. J. Almario et al., Root-associated fungal microbiota of nonmycorrhizal Arabis alpina and its contribution to plant phosphorus nutrition. Proceedings of the National Academy of Sciences 114, E9403-E9412 (2017).

48. C. Dietzen et al., The Transcription Factor EIL1 Participates in the Regulation of Sulfur-Deficiency Response. Plant Physiol 184, 2120-2136 (2020).

49. S. Hou et al., A microbiota–root–shoot circuit favours Arabidopsis growth over defence under suboptimal light. Nature Plants 7, 1078-1092 (2021).

50. P. Durán et al., Microbial Interkingdom Interactions in Roots Promote Arabidopsis Survival. Cell 175, 973-983.e914 (2018).

51. E. Bolyen et al., Reproducible, interactive, scalable and extensible microbiome data science using QIIME 2. Nature Biotechnology 37, 852-857 (2019).

52. T. Rognes, T. Flouri, B. Nichols, C. Quince, F. Mahé, VSEARCH: a versatile open source tool for metagenomics. PeerJ 4, e2584 (2016).

53. C. Quast et al., The SILVA ribosomal RNA gene database project: improved data processing and web-based tools. Nucleic Acids Res 41, D590-596 (2013).

54. R. H. Nilsson et al., The UNITE database for molecular identification of fungi: handling dark taxa and parallel taxonomic classifications. Nucleic Acids Research 47, D259-D264 (2018).

55. M. Nakata, M. Ohme-Takagi, Quantification of Anthocyanin Content. Bio-protocol 4, e1098 (2014).

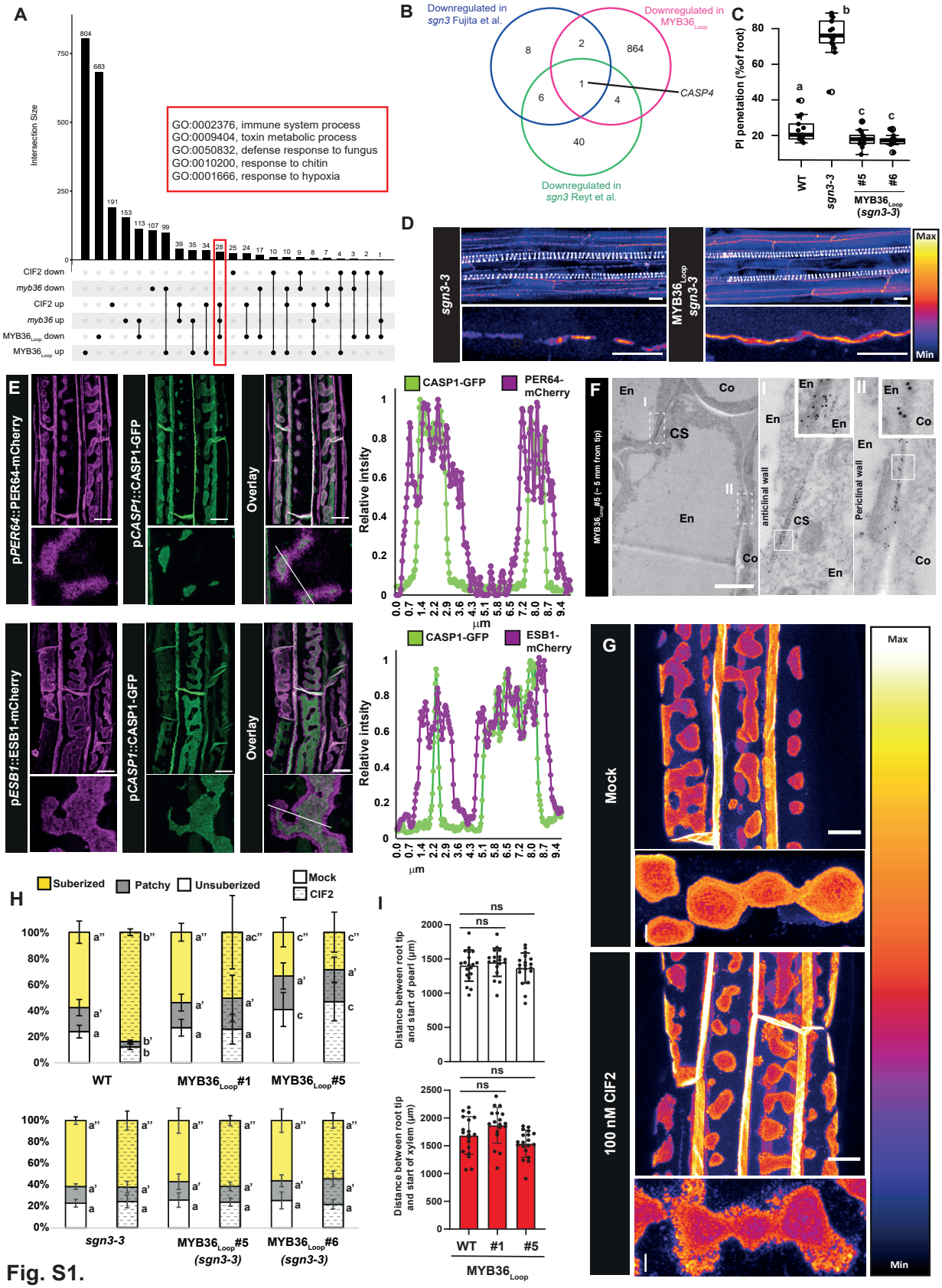

Fig. S1.

(A) Upset plot showing the number of differentially expressed genes (DEGs) in MYB36Loop #5 and myb36-2 roots grown on standard ½ MS agar medium, comparing with the DEGs in Col-0 roots treated with CIF2 from (9). (B) Venn diagram showing the overlap of downregulated genes in MYB36Loop#5 roots, downregulated genes in sgn3-3 roots from (14) and downregulated genes in Col-0 roots treated with CIF2 (9). (C) Measurement of the percentage of roots can be penetrated by propidium iodide (PI). Plants were grown on standard ½ MS agar medium for 7 days. (D) Maximum projection of a confocal image stack of Basic fuchsin-stained 7-day-old roots. Scalebars in upper images represent 10 µm whereas scalebars in lower images represent 5 µm (E) Maximum projection of a confocal image stack of 7-day-old roots, lines in overlay depict the transect used for relative intensity measurements. Scalebars represent 10 µm. (F) Transmission electron microscopy (TEM) micrograph of 7-day-old anti-GFP immunogold-labeled roots. Scalebar represents 500 nm. Co; Cortex, CS; Casparian strip, En: Endodermis. (G) Top-view maximum projection of 7-day-old MYB36Loop#5 plants treated with 100 nM CIF2 for 24h before fixing in Clearsee and imaged using a confocal setup. Scalebars represent 10 µm. (H) Measurement of suberization pattern under mock or 100 nM CIF2 conditions. (I) Bar plots showing the distance between root tip and start of pearl of string (top) and the distance between root tip and start of xylem (bottom). Plants were grown on standard ½ MS agar medium for 8 days. Data are mean ± SD. Statistical significance of differences with the parental line (WT) was determined using a two-tailed Student's t-test. ns; not significant. For boxplots, the center line in the box indicates the median, dots represent data, the box limits represent the upper and lower quartiles, and the whiskers represent the maximum and minimum values. Different letters depict statistical difference in a one-way ANOVA analysis with Tukey's test ($P < 0.05$).

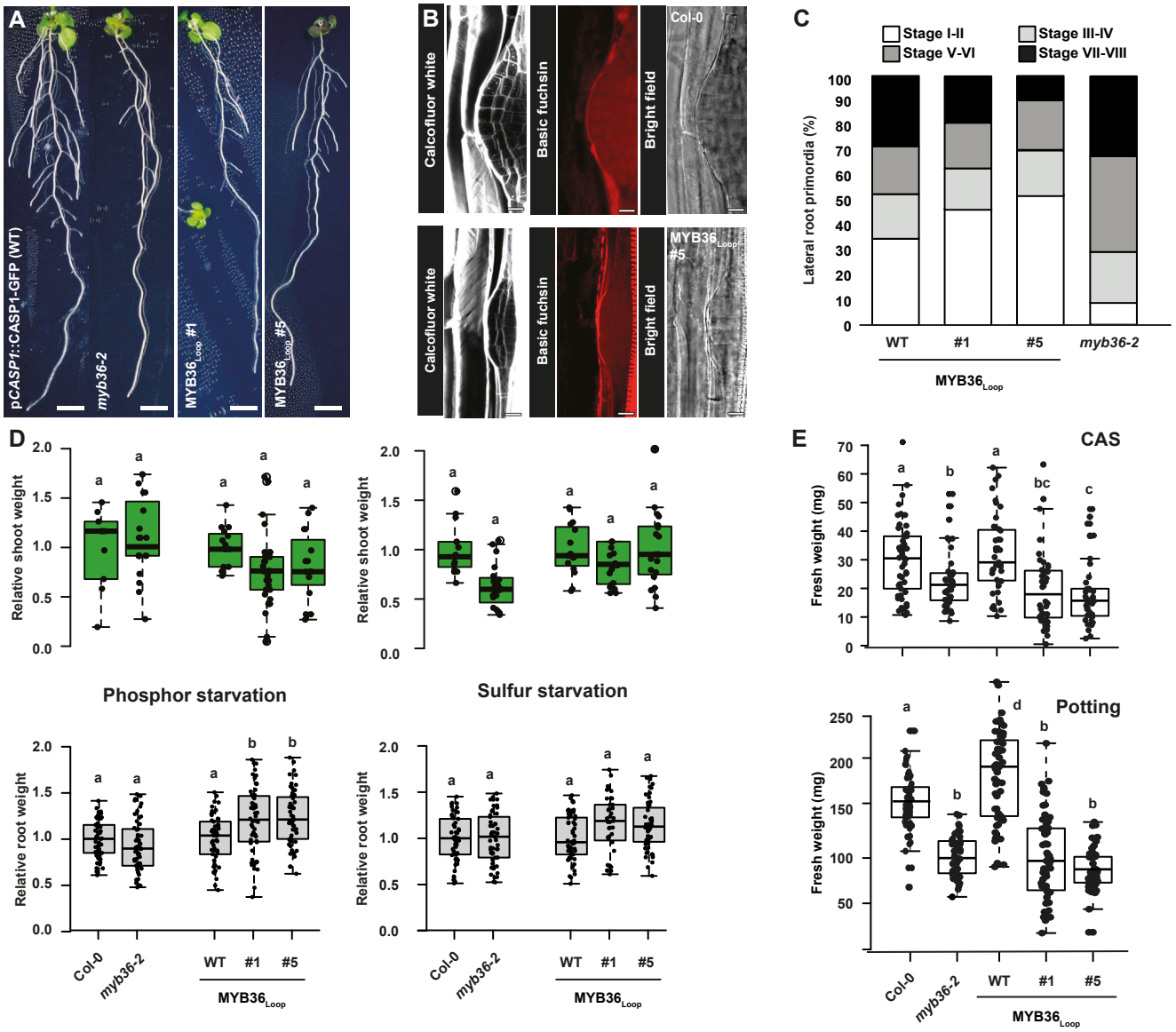

Fig. S2.

(A) 14-day-old seedlings grown on standard ½ MS agar medium. Scalebars represent 5 mm. (B) Lateral root primordia (LRP) of 8-day-old Col-0 (upper graph) and MYB36Loop#5 roots grown on standard ½ MS agar medium, stained with cell wall dye Calcofluor white and the lignin-specific dye Basic fuchsin. Scalebars represent 10 μm. (C) The distribution of different stages of LRP of 8-day-old plants grown on standard ½ MS agar medium. (D) Measurement of shoot (upper graph) and root (lower graph) fresh weight of 2-week-old plants grown under phosphor (left) or sulfur (right) starvation conditions. The weight was normalized to the changes in the corresponding parental background (Col-0 for myb36-2 and pCASP1::CASP1-GFP for MYB36Loop lines). (E) Measurement of shoot fresh weight of 4-week-old plants grown under CAS (upper) or standard potting soil (lower) conditions. For boxplots, the center line in the box indicates the median, dots represent data, the box limits represent the upper and lower quartiles, and the whiskers represent the maximum and minimum values. Different letters depict statistical difference in a one-way ANOVA analysis with Tukey's test ($P < 0.05$).

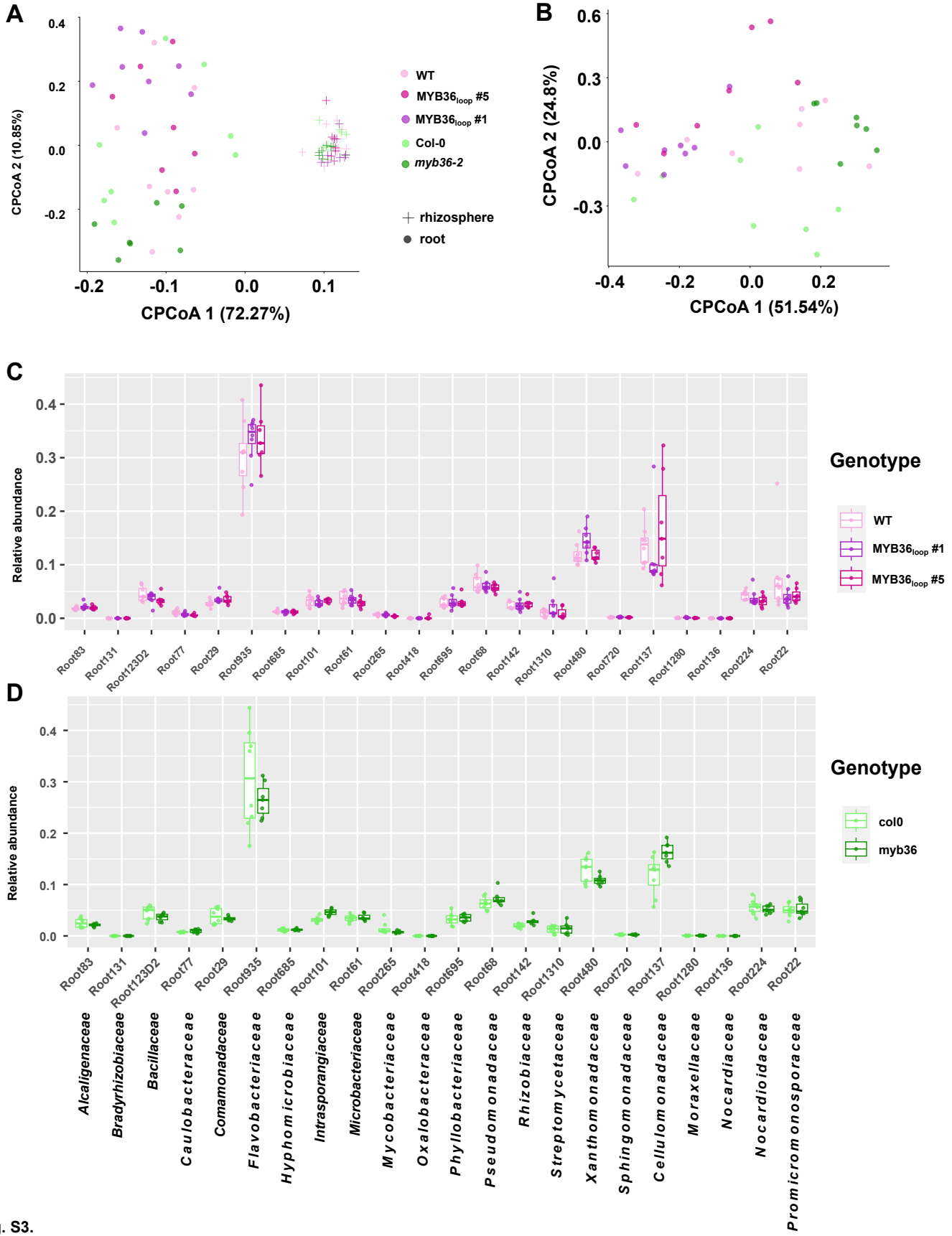

Fig. S3.

(A) Constrained Principal Coordinates Analysis (CPCoA) of Bray-Curtis dissimilarities of 16S amplicon reads from root and rhizosphere samples (41.7% of variance explained by genotype x compartment, P=0.001, PERMANOVA). (B) CPCoA of root samples only (17.8% of variance explained by genotype, P=0.003, PERMANOVA). (C and D) Relative abundance of individual SynCom strains (IDs shown as x-axis labels, and corresponding bacterial families below) in root samples of pCASP1::-CASP1-GFP (WT), MYB36Loop#1 and MYB36Loop#5 (C), and of Col-0 and myb36-2 (D).

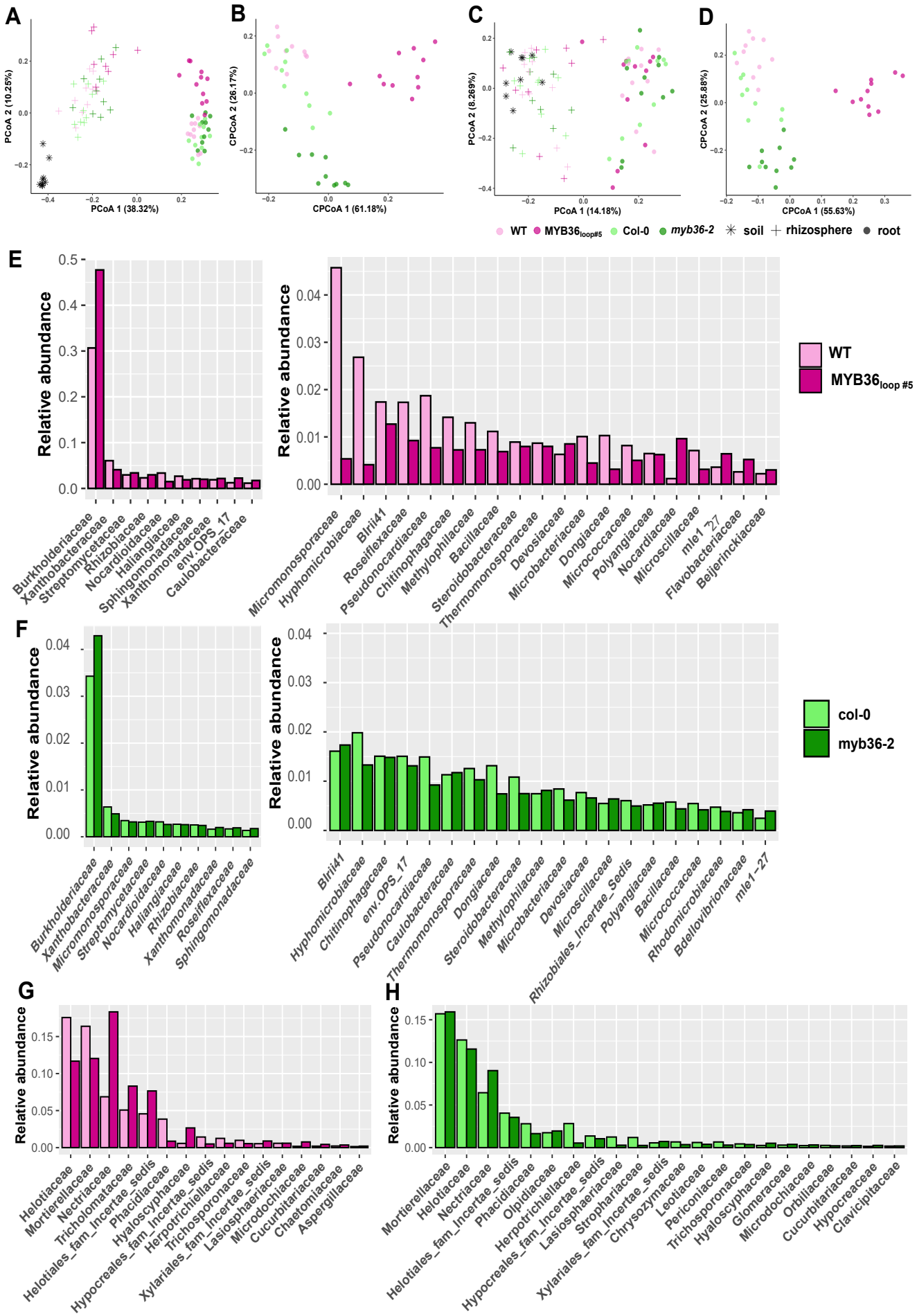

Fig.S4.

(A and C) PCoA of Bray-Curtis dissimilarities of bacterial 16S amplicon reads (A) and fungal ITS amplicon reads (C) from pCASP1::CASP1-GFP (WT), MYB36Loop #5, Col-0, and myb36-2 root and rhizosphere samples as well as unplanted soil samples. (B and D) Constrained PCoA of the same root samples, where 15.9% and 9.3% of the variance are explained by genotype for bacteria (B) and fungi (D), respectively (P=0.001, PERMANOVA). (E-H) Rank plot of median relative abundances of abundant bacterial (E and F) and fungal (G and H) families in MYB36Loop #5 and myb36-2 roots and their corresponding parental lines.

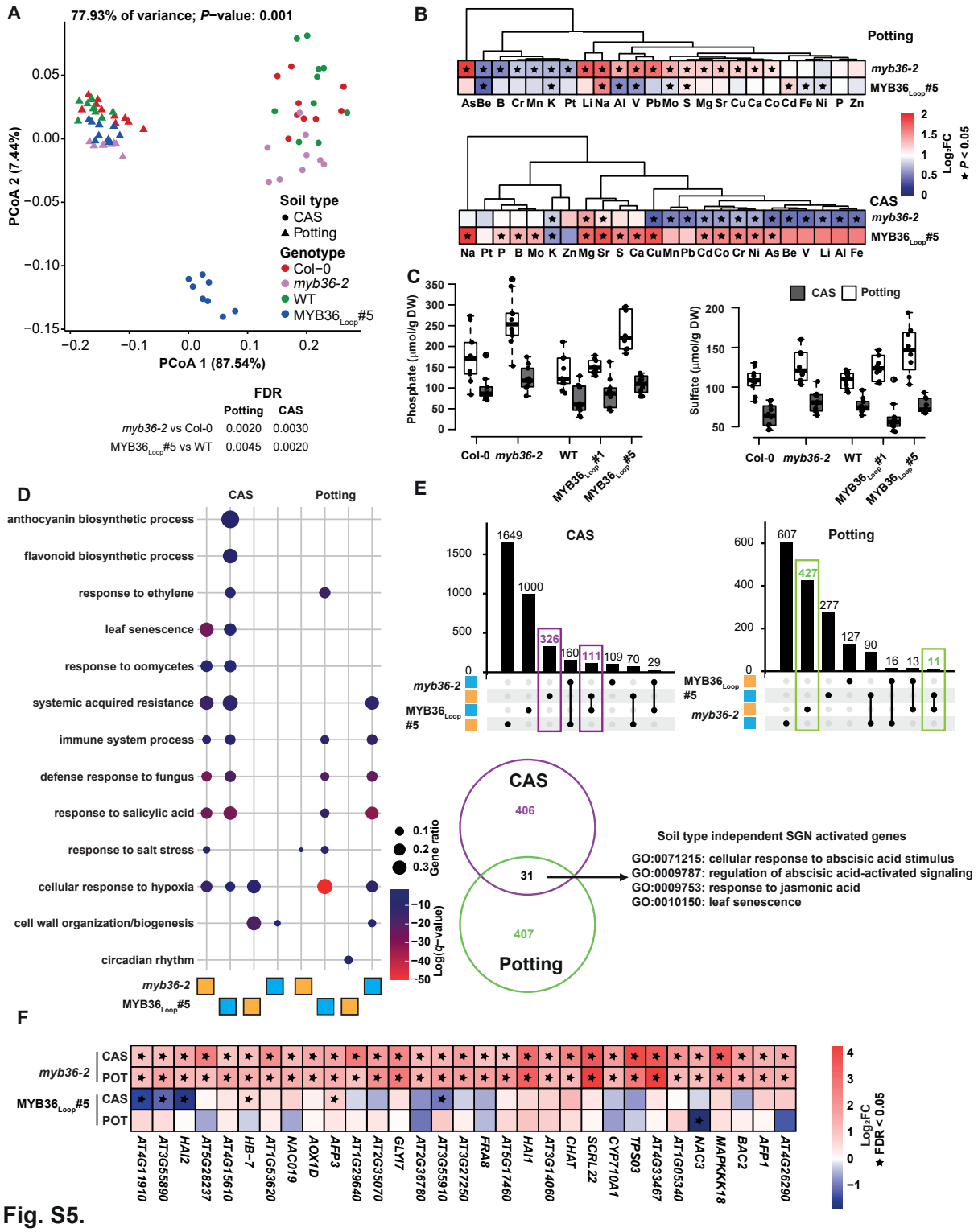

Fig. S5.

(A) PCoA plot of Bray-Curtis distances calculated on 24 shoot mineral contents of 4-week-old plants grown under CAS or standard potting soil conditions. 77.93% variation in shoot ionome can be explained by soil type. The lower table shows the statistical differences using permutational multivariate analysis of variance (PERMANOVA). (B) Heatmap of 24 element contents in 4-week-old MYB36Loop#5 and myb36-2 rosettes grown under standard potting soil (upper graph) or CAS (lower graph) conditions after normalization to the corresponding parental line. Star symbols represent significant differences with respective wild-type determined using a two-tailed Student's t-test (P < 0.05). (C) Measurement of phosphate (left graph) and sulfate (right graph) content in 4-week-old rosettes grown under CAS or standard potting soil conditions. (D) Gene Ontology (GO) term enrichment analysis of differentially expressed genes (DEGs) in rosettes of 4-week-old plants grown under CAS (left) or standard potting soil (right) conditions. Gene ratio represents the number of DEGs belonging to a certain GO term divided by the total gene number of this GO term. Orange: upregulated; blue: downregulated. (E) Upset plots (upper graph) showing the number of DEGs in MYB36Loop #5 and myb36-2 rosettes grown under CAS (left) or standard potting soil (right) conditions. Venn diagram (lower graph) indicating the 31 SGN-activated genes independent of soil type, and the GO terms enriched. (F) Heatmap indicating the 31 genes activated by SGN pathway independent of soil type. Star symbols represent significantly differentially expressed (FDR < 0.05) genes in MYB36Loop#5 and myb36-2 rosettes grown under CAS or standard potting soil (POT) conditions compared with the corresponding parental line. For boxplots, the center line in the box indicates the median, dots represent data, the box limits represent the upper and lower quartiles, and the whiskers represent the maximum and minimum values. SGN: Schengen.